

FULL PAPER

Highly selective and recyclable hydrogenation of α -pinene catalyzed by ruthenium nanoparticles loaded on amphiphilic core-shell magnetic nanomaterials

Fang-Zhu Wu¹ | Feng-Li Yu¹ | Bing Yuan¹ | Cong-Xia Xie^{1,2}  | Shi-Tao Yu³

¹State Key Laboratory Base of Eco-chemical Engineering, College of Chemistry and Molecular Engineering, Qingdao University of Science and Technology, Qingdao 266042, China

²Key Laboratory of Biomass Energy and Material, Jiangsu, Province, Nanjing 210042, China

³College of Chemical Engineering, Qingdao University of Science and Technology, Qingdao 266042, China

Correspondence

Feng-Li Yu, State Key Laboratory Base of Eco-chemical Engineering, College of Chemistry and Molecular Engineering, Qingdao University of Science and Technology, Qingdao, 266042, China.
Email: yufliqust@163.com

Cong-Xia Xie, Key Laboratory of Biomass Energy and Material, Jiangsu, Province, Nanjing 210042, China.
Email: xiecongxia@126.com

Funding information

Open Project of the Chemistry Department in Qingdao University of Science and Technology of China, Grant/Award Number: QUSTHX201811; Open Project of Jiangsu Key Laboratory of Biomass Energy and Material, Grant/Award Number: JSBEM201901; Shandong Province Emphasis Development Plan, Grant/Award Number: 2017GGX70102; Taishan Scholar Foundation of Shandong Province of China, Grant/Award Number: ts201511033; National Natural Science Foundation of China, Grant/Award Number: 31270615

A multifunctional nanomaterial ($\text{Fe}_3\text{O}_4@\text{SiO}_2@\text{C}_x@\text{NH}_2$) comprising a magnetic core, a silicon protective interlayer, and an amphiphilic silica shell is successfully prepared. Ru nanoparticles catalyst loaded on $\text{Fe}_3\text{O}_4@\text{SiO}_2@\text{C}_x@\text{NH}_2$ is used in hydrogenation of α -pinene for the first time. The novel nanomaterial with amphiphathy can be used as a solid foaming agent to increase gas-liquid-solid three-phase contact and accelerate the reaction. Under the mild conditions (40 °C, 1 MPa H_2 , 3 h), 99.9% α -pinene conversion and 98.9% *cis*-pinane selectivity are obtained, which is by far the best results reported. Furthermore, the magnetic nanocomposite catalyst can be easily separated by an external magnet and reused nine times with high selectivity maintaining.

KEYWORDS

amphiphilic, core-shell magnetic nanomaterials, hydrogenation, Ru nanoparticles, α -Pinene

1 | INTRODUCTION

In recent years, magnetic nanomaterials have been widely applied in many important fields such as medicine control and storage, adsorption stripping, and catalysis, due to their easy separation, large specific surface area, interfacial effect, and mesoporous effect.^[1–4] Adjusting the hydrophilicity and hydrophobicity of magnetic materials is very important for their performance.^[5–7] Undoubtedly, amphiphilic magnetic materials are more attractive in some applications than hydrophilic or hydrophobic congeners. Hence, amphiphilic magnetic nanomaterials comprising a magnetic inner core and a functionalized outer shell are generally prepared^[8,9]

cis-Pinane is an important industrial intermediate that is typically applied in medicines, perfumes, and extraction.^[10–12] It is mainly prepared by selective hydrogenation of α -pinene.^[10] Metal nanoparticles exhibit excellent catalytic activity for the hydrogenation reaction owing to their quantum size and surface effect.^[11,13,14] To prevent the aggregation of metal nanoparticles, a stabilizer or supported catalyst is usually applied in the catalytic system.^[15,16] Touaibia's team has systematically studied solvent-free hydrogenation of pinenes over heterogeneous catalysts based on different active metals (Pd, Pt, Ru, and Rh) and supports (carbon, silica and alumina), and the results show Ru/C provides the best catalytic activity under 2.75 MPa H₂.^[17,18] Our research group has made some progress in the stabilization of metal nanoparticles by using some polymers such as PVA, F127, P123, and TPGS-1000 as stabilizers.^[19–22] A high catalytic activity can be achieved under mild conditions owing to the formation of hydrophobic micellar microreactors.^[23–25] However, the addition of these stabilizers may also lead to the formation of stable emulsions, resulting in difficulty in catalyst separation from the product.^[26,27]

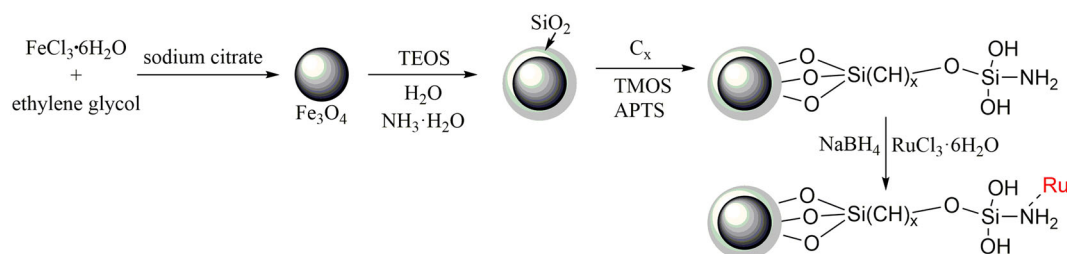
In this study, a multifunctional magnetic nanomaterial, Fe₃O₄@SiO₂@C_x@NH₂, comprising a magnetic inner core, SiO₂ protective interlayer, and alkyl-modified hydrophobic and NH₂-functionalized hydrophilic silica outer shell was successfully prepared. Ru nanoparticles stably loaded on Fe₃O₄@SiO₂@-

C_x@NH₂ were used for the first time to catalyze α -pinene hydrogenation. This novel nanomaterial with amphiphathy can be used as a solid foaming agent to increase the gas–liquid–solid three-phase contact and accelerate the reaction.^[28] The abundant –NH₂ groups in the outer shell allow the attachment of additional Ru nanoparticles.^[29,30] Furthermore, the magnetic nanocomposite catalyst can be easily separated using an external magnet. Therefore, the novel catalyst Fe₃O₄@SiO₂@C_x@NH₂/Ru exhibits an excellent catalytic activity, a high selectivity, and good recyclability in the hydrogenation of α -pinene under mild conditions, which are by far the best results reported.

2 | RESULTS AND DISCUSSION

Scheme 1 illustrates the overall preparation procedure of the target catalyst. The magnetic Fe₃O₄ inner core was firstly prepared via the redox method, and then wrapped with an SiO₂ layer using the microemulsion method. The SiO₂ layer was mainly used to prevent the corrosion of Fe₃O₄ and promote the dispersion of nanoparticles. Subsequently, an alkyl-modified hydrophobic silica and NH₂-functionalized hydrophilic silica outer shell were prepared. Finally, the insitu reduction of an Ru precursor by NaBH₄ produced the target catalyst Fe₃O₄@SiO₂@C_x@NH₂/Ru.

TEM images of the Fe₃O₄ core, Fe₃O₄@SiO₂, and Fe₃O₄@SiO₂@C₁₂@NH₂ (Figures S1–S3) clearly show that the prepared nanoparticles have a uniform spherical structure, and that the average particle sizes are 51.2, 223.5, and 325 nm, respectively (determined using a Malvern particle size analyzer) (Figures S4–S6). Particles between 300 and 350 nm in size account for approximately 70% of the prepared Fe₃O₄@SiO₂@C₁₂@NH₂. Figure 1 shows the high-angle annular dark-field scanning TEM (STEM) and the corresponding energy-dispersive X-ray spectroscopy (EDX) elemental mapping images of the target nanocomposite catalyst Fe₃O₄@SiO₂@C₁₂@NH₂/Ru. The STEM-EDX images clearly display the distribution of Fe, Si, and Ru elements. The results confirmed that the magnetic core, silica outer



SCHEME 1 Preparation of Fe₃O₄@SiO₂@C_x@NH₂/Ru catalyst.

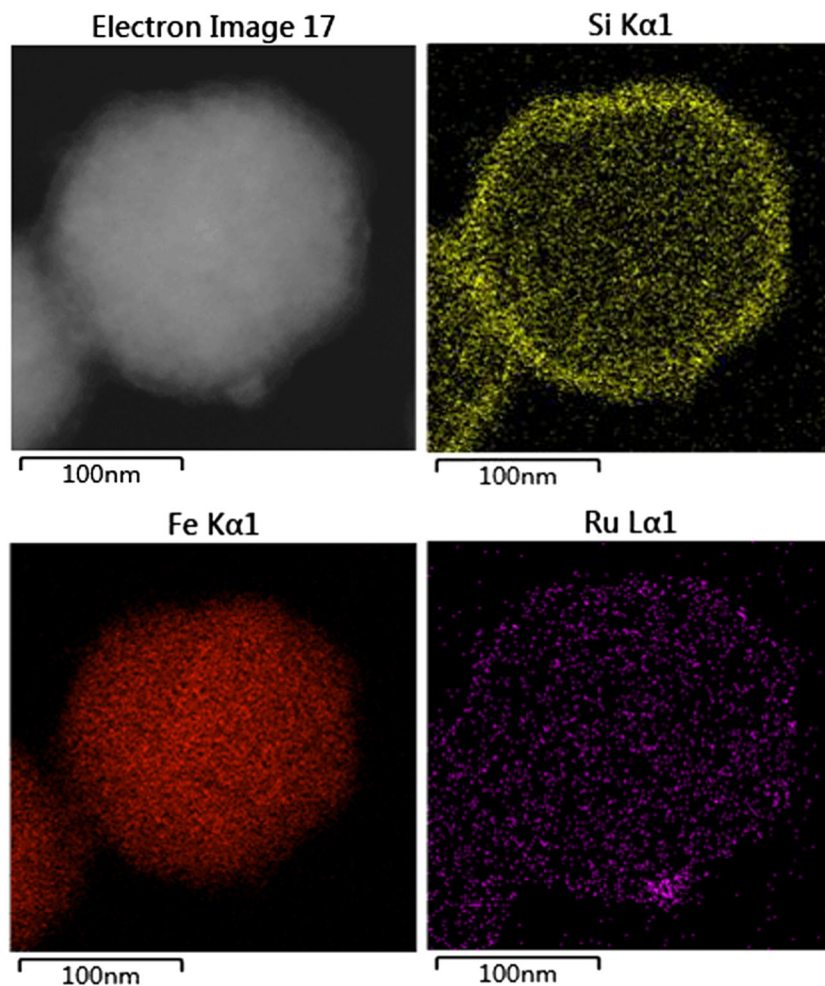


FIGURE 1 STEM-EDX images of $\text{Fe}_3\text{O}_4@SiO_2@C_{12}@NH_2/Ru$

shell, and Ru atoms were uniformly immobilized on the magnetic nanomaterial, thus indicating that Ru existed in the nanoparticles rather than in the aggregates.

In the FT-IR spectrum of $\text{Fe}_3\text{O}_4@SiO_2@C_{12}@NH_2/Ru$ (Figure 2), the absorption peaks of 452 and 1050 cm^{-1} respectively corresponded to the stretching vibrations of Fe-O bond and Si-O-Si band, which showed that SiO_2 was successfully coated on the magnetic core. The characteristic absorption peaks at 2853 and 2923 cm^{-1} showed that the hydrophobic group C_{12} was successfully introduced in the silica. The broad peak at 3400 cm^{-1} was the stretching vibration peak of N-H bond, indicating that the hydrophilic functional group $-NH_2$ was also grafted on the silica shell.

The unique hydrophilicity/hydrophobicity of the prepared magnetic nanomaterial was also examined by the measurement of the water droplet contact angle (Figure S7). The results indicated that the water droplet contact angle was approximately 47.5° for $\text{Fe}_3\text{O}_4@SiO_2@C_{12}@NH_2/Ru$, and but the water droplet contact angle of $\text{Fe}_3\text{O}_4@SiO_2@C_{12}/Ru$ was 99.5° , thus revealing the fact that the NH_2 -modified magnetic nanomaterial was amphiphilic.

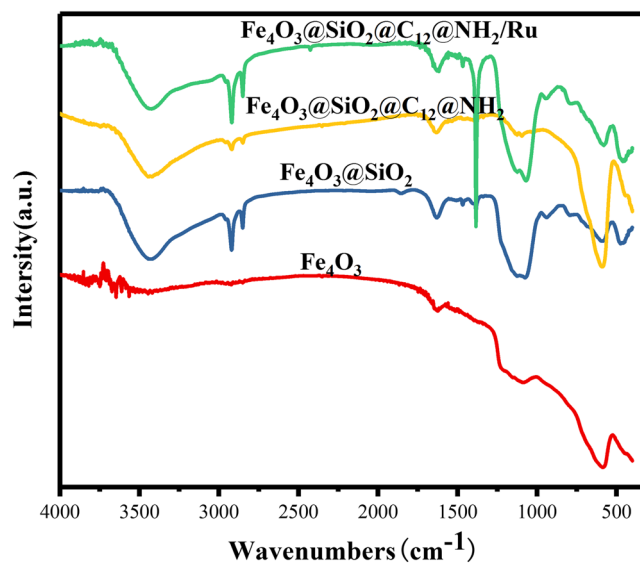


FIGURE 2 FT-IR spectrum of $\text{Fe}_3\text{O}_4@SiO_2@C_{12}@NH_2/Ru$

The zeta potential of $\text{Fe}_3\text{O}_4@SiO_2@C_{12}@NH_2/Ru$ in aqueous solution was examined and yielded a value of $+36.7\text{ mV}$ that confirmed a good dispersion stability of the prepared catalyst in water. However, when applying

an external magnetic field, the catalyst can be well gathered and recovered (Figure 3). Field-dependent magnetic characterizations of different nanoparticles were measured using a magnetic property measurement system (MPMS) magnetometer at 300 K, and the results showed that Fe_3O_4 nanoparticles, $\text{Fe}_3\text{O}_4@/\text{SiO}_2$, and $\text{Fe}_3\text{O}_4@/\text{SiO}_2@/\text{C}_{12}/\text{NH}_2/\text{Ru}$ nanocomposite have magnetization saturation values of 82.1, 41.5, and 21.12 emu g^{-1} , respectively (Figure 4). Although there is a decline of magnetization saturation value after the progressive modification of Fe_3O_4 nanoparticles, an easy separation of the catalyst from its dispersed aqueous solution within a few minutes can be achieved by simply using an external magnet. What's more, the amphiphilic shell can prevent the irreversible aggregation of magnetic particles after removal of the magnetic field.

The wide-angle XRD patterns of various nanomaterials are shown in Figure 5. A series of diffraction peaks at $2\theta = 30.26, 35.68, 43.32, 57.3$ and 62.84° are attributed to Fe_3O_4 nanoparticles. The diffraction peak near $2\theta = 23^\circ$ is characteristic for amorphous SiO_2 . For the XRD pattern of $\text{Fe}_3\text{O}_4@/\text{SiO}_2@/\text{C}_{12}/\text{NH}_2/\text{Ru}$, it displays the characteristic diffraction peaks of both the magnetite phase and the amorphous silica. However, there is no the characteristic of Ru crystals, indicating that Ru is highly dispersed and exists in the nanoparticles rather than in aggregated forms.

XPS characterization of $\text{Fe}_3\text{O}_4@/\text{SiO}_2@/\text{C}_{12}/\text{NH}_2/\text{Ru}$ is afforded. In the full spectrum (Figure S8), the binding energies of Ru $3\text{P}_{1/2}$, Ru $3\text{P}_{3/2}$ and Ru $3\text{d}_{5/2}$ are located at 484.5, 462.5 and 280.4 eV, respectively, which is consistent with the standard spectrum of Ru. From the partial enlargement of Ru 3d, 67.8% of Ru was reduced to Ru(0) in the zero valence state (Figure S9). The binding energy changes of the C, O, and N atoms before and after the loading of Ru nanoparticles were also detected by XPS. The binding energies of the C and O atoms elicit

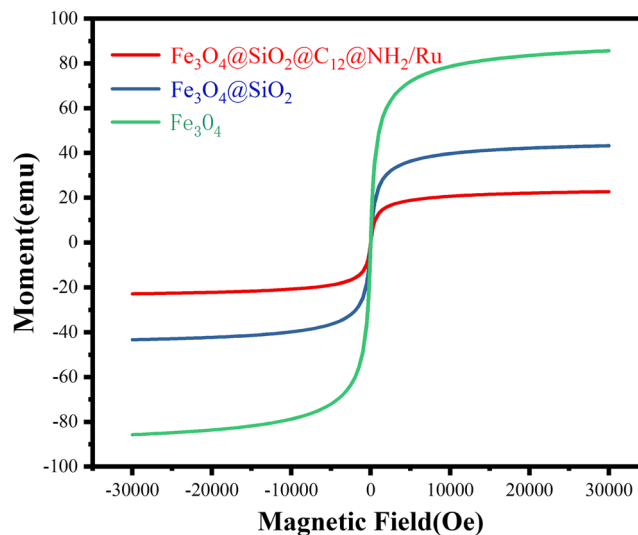


FIGURE 4 Magnetic hysteresis loops of nanoparticles recorded at 25 °C

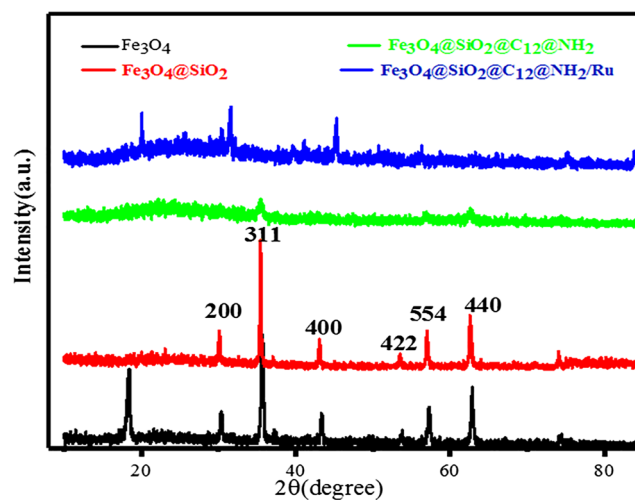


FIGURE 5 Wide-angle XRD patterns of various nanomaterials

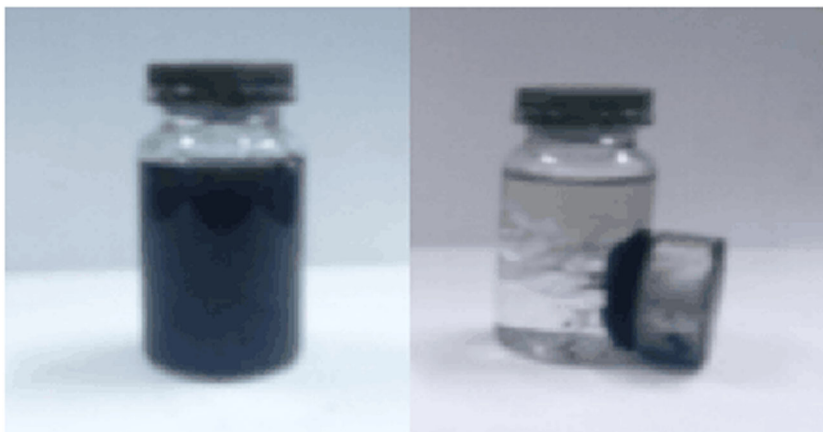


FIGURE 3 Dispersion and separation of $\text{Fe}_3\text{O}_4@/\text{SiO}_2@/\text{C}_{12}/\text{NH}_2/\text{Ru}$

no any changes (Figures S10 and S11). However, $\Delta E = 1.96$ eV is observed for the N atoms (Figure S12), which demonstrates that Ru nanoparticles are mainly bonded to $-\text{NH}_2$ on the surface of the nanomaterial.

- The prepared magnetic nanomaterial catalysts were used to catalyze the hydrogenation of α -pinene. According to the entries 1–3 in Table 1, the modification of different carbon chains on $\text{Fe}_3\text{O}_4@ \text{SiO}_2@ \text{C}_x@ \text{NH}_2/\text{Ru}$ has a considerable influence on the catalytic hydrogenation. N_2 adsorption–desorption isotherms in Figure S13 show typical type IV adsorption–desorption isotherm characteristics with specific surface areas of 18.19, 31.67, and 53.30 m^2/g for C_8 , C_{12} and C_{18} -modified catalysts, respectively. The BJH pore size distribution curves in Figures S14 and S15 show that the pore diameters of C_{18} and C_{12} -modified catalysts are up to 7.55 and 3.58 nm, respectively. However, C_8 -modified catalyst has a non-uniform pore size distribution (Figure S16), resulting in a poor loading of Ru nanoparticles. Another, shorter carbon chain with relatively low hydrophobicity is not conducive to the dispersion of the catalyst in the water–organic system. The larger specific surface area and uniform pore diameter benefit the loading of Ru nanoparticles. However, longer carbon chains with a larger steric hindrance are unfavorable to the contacts of the substrate with Ru nanoparticles. Therefore, C_{12} -modified catalyst with optimal amphiphaticity exhibits the best catalytic activity (entry 2). By comparison of Pd, Co, and Ni with Ru nanoparticles (entries 4–6), Ru nanoparticles exhibit the highest catalytic activity, and can high-efficiently convert α -pinene to *cis*-pinane under the mild conditions. Compared with non-amphiphilic magnetic materials (entries 7 and 8), magnetic amphiphilic catalysts have higher catalytic activity,

indicating that amphiphilicity is of great significance for heterogeneous hydrogenation. Therefore, under the same conditions, compared with Pd/C and Ru/C (entries 9 and 10), $\text{Fe}_3\text{O}_4@ \text{SiO}_2@ \text{C}_{12}@ \text{NH}_2/\text{Ru}$ catalyst is used to catalyze the hydrogenation of α -pinene with obvious advantages.

For the hydrogenation of α -pinene catalyzed by $\text{Fe}_3\text{O}_4@ \text{SiO}_2@ \text{C}_{12}@ \text{NH}_2/\text{Ru}$ in the aqueous solution, the reaction conditions including catalyst dosage, water volume, H_2 pressure, reaction temperature, and the reaction time, were all optimized (Figures S17–21). The results showed the best hydrogenation conditions were as follows: a catalyst mass equal to 7 mg, water volume 20 mL, a H_2 pressure of 1 MPa, a reaction temperature equal to 40 °C, and a reaction time of 3 hr. The α -pinene was completely converted with a *cis*-pinane selectivity of 99%.

Except for the high catalytic activity, another great advantage of the novel magnetic catalyst is its easy separation from the reaction system. After the reaction, the magnetic catalyst can be easily separated by an external magnet, and reused to the next reaction. Under the optimum reaction conditions, the recyclability of the magnetic catalyst for the hydrogenation of α -pinene is shown in Figure 6. The conversion and selectivity have no obvious change during five recycling times. After that, the conversion becomes have a little drop, meanwhile, the high selectivity still maintains. However, when the catalyst is reused eight times, the conversion of α -pinene is still higher than 85%. From the TEM of the catalyst after 8th reuse, the morphology and structure of the catalyst are unchanged. Compared to the fresh catalyst, the loss of Ru nanoparticles was only 0.15 wt% according to ICP-AES analysis after eight cycles, indicating that Ru nanoparticles were stably loaded on the nanomaterial. Therefore, the decline of α -pinene conversion probably owes to the carbon deposition in the holes of the molecular sieves.

TABLE 1 Catalytic activity of different modified catalysts^[a]

Entry	Catalyst	Conversion/%	Selectivity/%
1	$\text{Fe}_3\text{O}_4@ \text{SiO}_2@ \text{C}_8@ \text{NH}_2/\text{Ru}$	80.2	98.7
2	$\text{Fe}_3\text{O}_4@ \text{SiO}_2@ \text{C}_{12}@ \text{NH}_2/\text{Ru}$	99.9	98.9
3	$\text{Fe}_3\text{O}_4@ \text{SiO}_2@ \text{C}_{18}@ \text{NH}_2/\text{Ru}$	85.2	98.5
4	$\text{Fe}_3\text{O}_4@ \text{SiO}_2@ \text{C}_{12}@ \text{NH}_2/\text{Pd}$	68.7	84.4
5	$\text{Fe}_3\text{O}_4@ \text{SiO}_2@ \text{C}_{12}@ \text{NH}_2/\text{Co}$	32.1	52.7
6	$\text{Fe}_3\text{O}_4@ \text{SiO}_2@ \text{C}_{12}@ \text{NH}_2/\text{Ni}$	47.5	68.9
7	$\text{Fe}_3\text{O}_4@ \text{SiO}_2@ \text{C}_{12}/\text{Ru}$	32.4	98.6
8	$\text{Fe}_3\text{O}_4@ \text{SiO}_2@ \text{NH}_2/\text{Ru}$	52.4	85.4
9	Pd/C	28.3	92.7
10	Ru/C	18.9	31.4

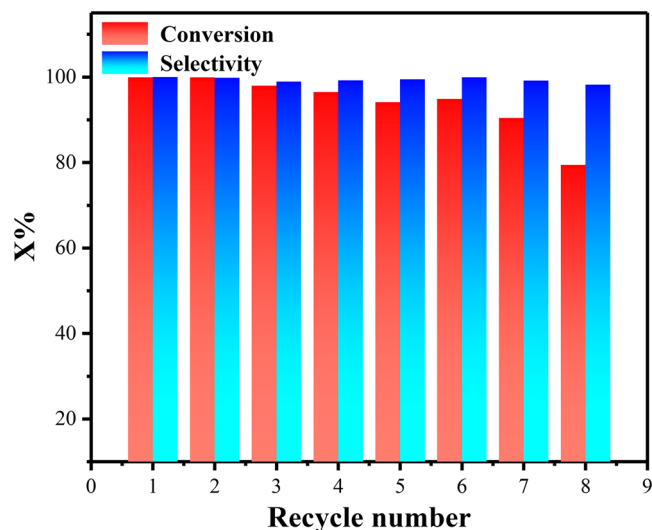


FIGURE 6 Recyclability of the catalyst (40 °C, 1 MPa, 3 hr)

As Figure 7, the microscopic image of H₂ bubbles in the oil–water biphasic interface for the novel catalytic system clearly showed that the bubbles gradually migrated into the oil phase from the water phase, became small and gradually broke. The released hydrogen then reacted with α -pinene in the oil phase on the surface of the solid catalyst. The catalytic reaction proceeded at the gas–liquid–solid interface. The novel amphiphathy nanomaterial can be used as a solid foaming agent to increase gas–liquid–solid three-phase contact and further accelerate the reaction. What's more, every nanocomposite is equivalent to a microreactor. Therefore, for the novel catalytic system, the hydrogenation reaction has a

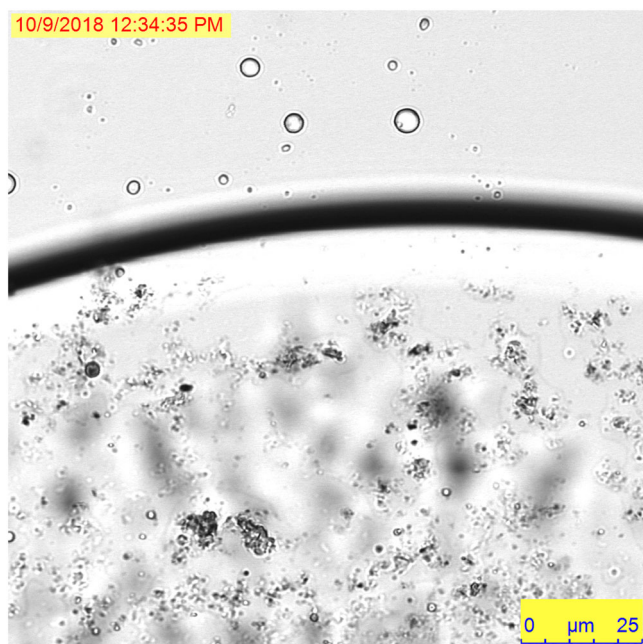


FIGURE 7 Microscopic image of H₂ bubbles in oil–water biphasic interface

lower activation energy, and H atoms are more easily added to the double bond of α -pinene under the mild hydrogenation condition. Additionally, the steric hindrance of the nanocomposite allows only the endo-surface of the α -pinene to contact with the Ru nanoparticle catalyst, resulting in a high selectivity for *cis*-pinene.

In addition to α -pinene, the novel catalytic hydrogenation system can be applied to many other unsaturated compounds, including alkenes and aromatic compounds, as shown in Table 2. Under mild conditions, these unsaturated compounds can all be very efficiently hydrogenated. Therefore, the novel catalyst has a wide application field.

3 | EXPERIMENTAL

3.1 | Chemicals and reagents

Hexadecyl trimethyl ammonium bromide (CTAB), octyl trimethoxysilane (C₈), dodecyl trimethoxysilane (C₁₂), 3-aminopropyl trimethoxysilane (APTS), and hydrated ruthenium trichloride (RuCl₃·3H₂O) were purchased from the Aladdin Industrial Corporation. Hydrated ferric trichloride (FeCl₃·6H₂O), trisodium citrate, sodium acetate, ethylene glycol, octadecyl trimethoxysilane (C₁₈), tetraethylsilane (TEOS), tetramethylsilane (TMOS), aqueous ammonia (NH₃·H₂O, 28 wt%), sodium hydroxide (NaOH), and sodium borohydride (NaBH₄) were obtained from Shanghai Macklin Biochemical Technology Co.,

TABLE 2 Hydrogenation of unsaturated compounds using the new catalytic system

Substrate	Product	P/ MPa	T/ °C	t/ min	Conversion/%
		1	35	60	99.89
		1	35	60	99.98
		1	30	40	99.95
		1	35	60	99.95
		1	35	60	99.96
		1	25	40	99.97
		1	25	40	99.99
		1	25	40	99.97
		1	30	40	99.98

LTD. Additionally, α -pinene (98%) was supplied by Guangxi Wuzhou Rosin Factory, and hydrogen (99.99 wt%) was obtained from Qingdao Airichem Specialty Gases & Chemicals Co., Ltd. All solvents were purchased and purified before use. Doubly deionized water was used in all experiments.

3.2 | Synthesis of Fe_3O_4 nanoparticles

The magnetic nanoparticles were synthesized through a solvothermal reaction according to the literature.^[31] The reaction system was isolated from moisture throughout the entire preparation process. $\text{FeCl}_3 \cdot 6\text{H}_2\text{O}$ (0.65 g) and trisodium citrate (0.26 g) were rapidly mixed and completely dissolved into ethylene glycol (20 ml), followed by the addition of sodium acetate (1.20 g). A homogeneous dark suspension was gotten after continuously stirring for 30 min, and then transferred into a teflon-lined autoclave and maintained at 200 °C for 10 hr. Cooled to ambient temperature, the black Fe_3O_4 nanoparticles were obtained after ethanol and water washing subsequently, and final vacuum drying.

3.3 | Synthesis of core-shell structured $\text{Fe}_3\text{O}_4@ \text{SiO}_2$

For the silica coating, Fe_3O_4 nanoparticles (400 mg) were first dispersed in a mixture of ethanol (60 ml) and deionized water (40 mL) by ultrasonication, and then aqueous ammonia solution (2 ml, 28 wt%) and TEOS (100 mg) were added sequentially. The mixture was stirred for 8 hr at room temperature to form a SiO_2 coating layer through condensation on the magnetic nanoparticles. The obtained core-shell $\text{Fe}_3\text{O}_4@ \text{SiO}_2$ nanoparticles were collected by using a magnet and washed several times with deionized water and ethanol.

3.4 | Synthesis of amphiphilic core-shell structured $\text{Fe}_3\text{O}_4@ \text{SiO}_2@ \text{C}_x@ \text{NH}_2$

In a typical synthesis, the core-shell $\text{Fe}_3\text{O}_4@ \text{SiO}_2$ nanoparticles (250 mg) were dispersed in a solution of deionized water (100 ml) and methanol (125 ml), and 625 μL of NaOH solution (1 mol L^{-1}) and CTAB (0.88 g) were added. The mixture was vigorously stirred at room temperature for 2 hr. 162 μL of octyl trimethoxysilane (C_8) was added into the above mixture and stirred for 1 hr. Then 358 μL of TMOS and 322 μL of APTS were dropwise added into the above solution. After that, the solution was further stirred for 12 hr and crystallized for another 12 hr. The white solid was obtained by an external

magnet and washed to be neutral with water and ethyl alcohol. The solid powder was then extracted with anhydrous ethanol 3 times to remove organic template agent CTAB at 80 °C for 12 hr every time. The formed precipitate was separated and desiccated to afford amphiphilic core-shell structured $\text{Fe}_3\text{O}_4@ \text{SiO}_2@ \text{C}_8@ \text{NH}_2$, $\text{Fe}_3\text{O}_4@ \text{SiO}_2@ \text{C}_{12}@ \text{NH}_2$ and $\text{Fe}_3\text{O}_4@ \text{SiO}_2@ \text{C}_{18}@ \text{NH}_2$ were prepared according to the same procedure, when octyl trimethoxysilane (C_8) was replaced by dodecyl trimethoxysilane (C_{12}) and octadecyl trimethoxysilane (C_{18}) respectively, meanwhile the dosage of TEOS in the previous step respectively was changed to 400 mg and 800 mg.

3.5 | Loading of Ru nanoparticles

Ruthenium nanoparticles were loaded on the prepared $\text{Fe}_3\text{O}_4@ \text{SiO}_2@ \text{C}_x@ \text{NH}_2$ by impregnation method. $\text{Fe}_3\text{O}_4@ \text{SiO}_2@ \text{C}_x@ \text{NH}_2$ (0.20 g) was first dispersed in 20 ml of ethyl alcohol, and $\text{RuCl}_3 \cdot 3\text{H}_2\text{O}$ (0.20 g) was added. The mixture was placed for 30 mins under ultrasonic. After that, NaBH_4 (10 ml, 1 mol L^{-1}) was slowly added into the above mixture under vigorous stirring. After stirring 4 hr at 40 °C, the black precipitate was collected by using a magnet, washed by ethyl alcohol, and dried under vacuum. The magnetic nanocomposite catalyst $\text{Fe}_3\text{O}_4@ \text{SiO}_2@ \text{C}_x@ \text{NH}_2/ \text{Ru}$ was afforded.

3.6 | Hydrogenation of α -pinene

In a typical reaction, α -pinene (1.0 g), the catalyst $\text{Fe}_3\text{O}_4@ \text{SiO}_2@ \text{C}_x@ \text{NH}_2/ \text{Ru}$ (20 mg), and 20 ml of H_2O were added into a 100 ml of high pressure reaction kettle. After sealing the kettle, the atmosphere in the kettle was replaced by 4 MPa H_2 4 times, and 1 MPa H_2 was finally filled. The mixture was stirred for 3 hr at 40 °C. After the reaction, the kettle was cooled to room temperature. The catalyst $\text{Fe}_3\text{O}_4@ \text{SiO}_2@ \text{C}_x@ \text{NH}_2/ \text{Ru}$ was recovered by using a magnet and reused. The product was collected by extraction with *n*-heptane, and analyzed by gas chromatography (GC).

3.7 | Measurements and characterization

The morphology of amphiphilic magnetic nanomaterial was determined with a JEOL JSM-6010LV scanning electron microscope (SEM) and a JEOL JEM-2100 transmission electron microscope (TEM). The high-angle, annular dark field scanning TEM (STEM), and the corresponding energy dispersive X-ray (EDX) elemental mapping images were recorded on TALOS F200X high

resolution TEM. FT-IR spectra were obtained using a Nicolet 510P FT-IR spectrometer with the KBr method (frequency range from 4000 to 400 cm^{-1}). The zeta potential was examined by a Nano S90 Malvern particle size analyzer. The water droplet contact angle was quantified by a JC2000 contact angle meter. XRD measurements were performed on a Rigaku D/max-2400 diffractometer when Cu-K α anode radiation was used as the X-ray source at 40 kV and 100 mA in the 2θ range of 0–80. The content of Ru was determined by using ICP-AES method which was running at 1200 W. Before the analysis, the catalyst was dissolved in a mixture of hydrofluoric acid and aqua regia. XPS data were recorded by using mono Al-K α as X-ray source and the hydrocarbon peak of C 1s at 284.60 eV was used to calibrate binding energies. The porous structure of the catalyst was measured by a Micromeritics ASAP 2020 N₂ adsorption–desorption isotherm at 77 K. Brunauer–Emmett–Teller (BET) surface areas were calculated from the linear part of the BET plot. Pore size distribution was estimated from the adsorption branch of the isotherm by the BJH method. The magnetic hysteresis loop of the catalyst was recorded by a MPMS3 magnetism performance measurement. Leica SP8 laser scanning confocal microscopy was used to study H₂ bubble images in the hydrogenation reaction. The hydrogenation product was analyzed by a GC-9790 gas chromatography instrument with a FID detector.

4 | CONCLUSION

Highly dispersed and stable catalysts comprising Ru nanoparticles supported on magnetic amphiphilic core-shell nanomaterial (Fe₃O₄@SiO₂@C_x@NH₂/Ru) are successfully prepared for use in hydrogenation of α -pinene for the first time. The abundant -NH₂ in the outer shell allows attaching more Ru nanoparticles. The novel nanomaterial with amphiphathy can be used as a solid foaming agent to increase gas–liquid–solid three-phase contact and accelerate the reaction, and every nanocomposite is equivalent to a microreactor. Furthermore, the magnetic nanomaterial can be easily separated by an external magnet and efficiently reused. Therefore, the novel catalyst of Fe₃O₄@SiO₂@C_x@NH₂/Ru exhibits an excellent catalytic activity, high selectivity, and good recyclability in the hydrogenation of α -pinene under the mild conditions. More importantly, except for α -pinene, the novel catalytic hydrogenation system can be applied to many others alkenes and aromatic compounds. The development of the novel magnetic amphiphilic nanomaterial is of great significance, and it shows a good application prospect.

ACKNOWLEDGMENTS

The authors are very grateful for the financial supports from the National Natural Science Foundation of China (31270615), the Taishan Scholar Foundation of Shandong Province of China (ts201511033), the Shandong Province Emphasis Development Plan (2017GGX70102), the Open Project of Jiangsu Key Laboratory of Biomass Energy and Material (JSBEM201901), and the Open Project of the Chemistry Department in Qingdao University of Science and Technology of China (QUSTHX201811).

ORCID

Cong-Xia Xie  <https://orcid.org/0000-0002-1209-2745>

REFERENCES

- [1] Y. J. Ai, Z. N. Hu, Z. X. Shao, L. Qi, *Nano Res.* **2018**, *11*, 287.
- [2] A. Maryam, K. Nadiya, K. Eskandar, *Appl. Organomet. Chem.* **2018**, *32*, 4346.
- [3] R. Liu, Y. L. Guo, G. Odusote, F. L. Qu, *ACS Appl. Mater.* **2013**, *5*, 9167.
- [4] H. H. Zai, Y. Z. Zhao, S. Y. Chen, L. Ge, *Nano Res.* **2018**, *11*, 2544.
- [5] Q. Zhang, X. Z. Shu, J. M. Lucas, F. D. Toste, G. A. Somorjai, A. P. Alivisatos, *Nano Lett.* **2013**, *14*, 379.
- [6] M. S. Islam, W. S. Choi, S. H. Kim, O. H. Han, H. J. Lee, *Adv. Funct. Mater.* **2015**, *25*, 6061.
- [7] H. B. Zou, R. W. Wang, Z. Q. Shi, J. Y. Dai, Z. T. Zhang, S. L. Qiu, *J. Mater. Chem. A* **2016**, *4*, 4145.
- [8] B. K. Kaang, N. Han, W. Jang, H. Y. Koo, *Chem. Eng. J.* **2018**, *331*, 290.
- [9] M. Esmaeilpour, S. Zahmatkesh, N. Fahimi, M. Nosratabadi, *Appl. Organomet. Chem.* **2018**, *32*, 4302.
- [10] N. Li, Q. F. Ma, W. Liu, Y. H. Lv, *Fine Chem.* **2010**, *11*, 1073.
- [11] S. B. Ren, J. H. Qiu, C. Y. Wang, B. L. Xu, Y. N. Fan, Y. Cen, *Chin. J. Inorg. Chem.* **2007**, *6*, 1021.
- [12] E. Y. Varón, A. Selka, A. S. Fabiano-Tixier, M. Balcells, R. C. Garayoa, A. Bily, M. Touaibia, F. Chemat, *Green Chem.* **2016**, *18*, 6596.
- [13] S. Tanielyan, N. Biunno, R. Bhagat, R. Augustine, *Top. Catal.* **2014**, *57*, 1564.
- [14] V. A. Semikolenov, I. Ilyna, I. L. Simakova, *Appl. Catal. A* **2001**, *211*, 91.
- [15] I. L. Simakova, Y. Solkina, I. Deliy, J. Warna, D. Y. Murzin, *Appl. Catal. A* **2009**, *356*, 216.
- [16] M. L. Casella, G. F. Santori, A. Moglioni, V. Vetere, J. F. Ruggera, G. M. Iglesias, O. A. Ferretti, *Appl. Catal. A* **2007**, *318*, 1.
- [17] A. Selka, N. A. Levesque, D. Foucher, O. Clarisse, F. Chemat, M. Touaibia, *Org. Process Res. Dev.* **2017**, *21*, 60.
- [18] F. J. N. Moutombi, A. Selka, A. S. F. Tixier, D. Foucher, O. Clarisse, F. Chemat, M. Touaibia, *C. R. Chim.* **2018**, *21*, 1035.

- [19] Y. H. He, S. Hwang, D. A. Cullen, M. A. Uddin, *Energy Environ. Sci.* **2019**, *12*, 250.
- [20] M. Zhao, C. H. Deng, X. M. Zhang, *Chem. Commun.* **2014**, 47, 1359.
- [21] S. L. Hou, X. Y. Wang, C. R. Huang, C. X. Xie, S. T. Yu, *Catal. Lett.* **2016**, *146*, 1.
- [22] S. L. Hou, C. X. Xie, F. L. Yu, B. Yuan, S. T. Yu, *RSC Adv.* **2016**, *6*, 54806.
- [23] S. L. Hou, C. X. Xie, H. Zhong, S. T. Yu, *RSC Adv.* **2015**, *5*, 89552.
- [24] X. Y. Wang, F. L. Yu, C. X. Xie, S. T. Yu, *Mol. Catal.* **2018**, *444*, 62.
- [25] X. Y. Feng, X. Y. Wang, D. Zhang, F. Feng, *Small* **2018**, *14*, 1703570.
- [26] L. H. Xie, X. Y. Wang, F. L. Yu, B. Yuan, *RSC Adv.* **2017**, *7*, 51452.
- [27] J. Y. Dai, H. B. Zou, R. W. Wang, Y. Wang, *Green Chem.* **2017**, *19*, 1336.
- [28] Y. Zhang, Q. Yue, L. Liu, X. Y. Yang, *Adv. Mater.* **2018**, *30*, 1800345.
- [29] Y. Liu, L. Li, S. W. Liu, C. X. Xie, *J. Mol. Catal. A-Chem.* **2016**, *424*, 269.
- [30] H. Veisi, S. B. Hemmati, P. Safarimehr, *J. Catal.* **2018**, *365*, 204.
- [31] S. R. Kandibanda, N. Gundeboina, S. Das, V. M. Sunkara, *J. Photochem. Photobiol. B* **2018**, *178*, 270.

SUPPORTING INFORMATION

Additional supporting information may be found online in the Supporting Information section at the end of the article.

How to cite this article: Wu F-Z, Yu F-L, Yuan B, Xie C-X, Yu S-T. Highly selective and recyclable hydrogenation of α -pinene catalyzed by ruthenium nanoparticles loaded on amphiphilic core-shell magnetic nanomaterials. *Appl Organometal Chem.* 2019;e5165. <https://doi.org/10.1002/aoc.5165>